Remote Sensing of Environment 115 (2011) 2836–2849

Contents lists available at ScienceDirect

Remote Sensing of Environment

journal homepage: www.elsevier.com/locate/rse

Impact of spatial variability of tropical forest structure on radar estimation of aboveground biomass

Sassan Saatchi [a,*], Miriam Marlier [b], Robin L. Chazdon [c], David B. Clark [d], Ann E. Russell [e]

[a] Jet Propulsion Laboratory, California Institute of Technology, Pasadena, CA 91109, USA
[b] Dept. of Atmospheric Sciences, University of California, Los Angeles, CA 90095, USA
[c] Department of Ecology and Evolutionary Biology, University of Connecticut, Storrs, CT 06269, USA
[d] International Center for Tropical Ecology, University of Missouri, USA
[e] Dep. of Natural Resource Ecology, and Management, Iowa State University, Ames, IA 50011, USA

ARTICLE INFO

Article history:
Received 31 May 2009
Received in revised form 20 April 2010
Accepted 12 July 2010
Available online 19 May 2011

Keywords:
Radar
Lidar
Biomass
Carbon
Forest structure
Tropical forests
Costa Rica
La Selva Biological Station
DESDynl
BIOMASS

ABSTRACT

Understanding the spatial variability of tropical forest structure and its impact on the radar estimation of aboveground biomass (AGB) is important to assess the scale and accuracy of mapping AGB with future low frequency radar missions. We used forest inventory plots in old growth, secondary succession, and forest plantations at the La Selva Biological Station in Costa Rica to examine the spatial variability of AGB and its impact on the L-band and P-band polarimetric radar estimation of AGB at multiple spatial scales. Field estimation of AGB was determined from tree size measurements and an allometric equation developed for tropical wet forests. The field data showed very high spatial variability of forest structure with no spatial dependence at a scale above 11 m in old-growth forest. Plot sizes of greater than 0.25 ha reduced the coefficients of variation in AGB to below 20% and yielded a stationary and normal distribution of AGB over the landscape. Radar backscatter measurements at all polarization channels were strongly positively correlated with AGB at three scales of 0.25 ha, 0.5 ha, and 1.0 ha. Among these measurements, PHV and LHV showed strong sensitivity to AGB$<$300 Mg ha^{-1} and AGB$<$150 Mg ha^{-1} respectively at the 1.0 ha scale. The sensitivity varied across forest types because of differences in the effects of forest canopy and gap structure on radar attenuation and scattering. Spatial variability of structure and speckle noise in radar measurements contributed equally to degrading the sensitivity of the radar measurements to AGB at spatial scales less than 1.0 ha. By using algorithms based on polarized radar backscatter, we estimated AGB with RMSE = 22.6 Mg ha^{-1} for AGB$<$300 Mg ha^{-1} at P-band and RMSE = 23.8 Mg ha^{-1} for AGB$<$150 Mg ha^{-1} at L-band and with the accuracy optimized at 1-ha scale within 95% confidence interval. By adding the forest height, estimated from the C-band Interferometry data as an independent variable to the algorithm, the AGB estimation improved beyond the backscatter sensitivity by 20% at P-band and 40% at L-band. The results suggested the estimation of AGB can be improved substantially from the fusion of lidar or InSAR derived forest height with the polarimetric backscatter.

1. Introduction

Tropical forests are among the most structurally complex and carbon-rich ecosystems in the world. This complexity is related both to the size–frequency distribution of woody stems (Clark & Clark, 2000; Denslow & Hartshorn, 1994) and to the three-dimensional arrangement of canopy elements (e.g., leaves, branches, trunks) from the top of the canopy to the ground (Richards, 1996). Fine-scale vertical and horizontal gradients in light availability, humidity, and temperature modify biological processes that control mortality, recruitment, competition, and growth rates, which further modify the spatial organization of forest structural components and species composition (Clark et al., 1996; Nicotra et al., 1999; Oberbauer et al., 1993; Rich et al., 1993). The aboveground biomass (AGB) of a forest stand is directly influenced by the complexity of forest structure in both horizontal and vertical dimensions. This complexity is related to disturbance intensity and history and spatial variations influenced by edaphic conditions of the forest (e.g. soil, topography) (Chazdon, 1996; Clark et al., 1998; Clark & Clark, 2000; Laurance et al., 1999). Knowledge of forest structure and biomass across landscapes can provide information about the magnitude of carbon stored in one of the largest terrestrial pools, and can be used to quantify the carbon flux caused by deforestation or natural disturbance and to model the exchange of energy and matter between the atmosphere and forests (Dixon et al., 1994; Perry, 1994).

* Corresponding author. Tel.: +1 818 354 1051; fax: +1 818 393 5184.
E-mail address: saatchi@congo.jpl.nasa.gov (S. Saatchi).

0034-4257/$ – see front matter © 2011 Elsevier Inc. All rights reserved.
doi:10.1016/j.rse.2010.07.015

Because biomass can only be measured directly through destructive sampling, it is usually estimated based on structural measurements such as tree diameter and height. Although field biomass estimation methods are useful for local-scale studies, other methods such as interpolation by geospatial analysis or remote sensing techniques are necessary for the inventory of biomass over extensive regions. In both cases, the underlying spatial variability of forest biomass must be assessed to permit accurate interpolation or estimation from remote sensing data. In most remote sensing techniques, an empirical correlation between estimated forest biomass and the measurement of a forest structural parameter (e.g. height, volume, crown size) or the intensity of EM energy (or the ratio of energy at different wavelengths) received by the instrument is the basis for estimation of biomass distribution over a region. Among remote sensing techniques, active sensors such as lidar and radar provide the measurements suitable to estimate biomass at various spatial scales (Drake et al., 2003; Saatchi & Moghaddam, 2000).

Here we investigate the sensitivity of radar backscatter measurements at two wavelengths to aboveground biomass of a Tropical Wet Forest in Costa Rica. We examine how the spatial variability of forest biomass and the intrinsic spatial and measurement errors in radar observations impact the accuracy and the spatial resolution of biomass estimation. The results are then discussed in the context of two new spaceborne missions, DESDynl and BIOMASS, designed by NASA and ESA (European Space Agency) respectively.

2. Study area and data

2.1. Study area

The La Selva Biological Station is located near the Sarapiquíı River in northeast Costa Rica (Fig. 1). Over its 46-year history, La Selva has become one of the most heavily studied tropical forests in the world (Clark, 1990; McDade et al., 1994). This 1536-ha area is composed of a mixture of lowland old-growth and secondary Tropical Wet Forest (Clark & Clark, 2000; Guariguata et al., 1997; Holdridge et al., 1971), abandoned pasture, current and abandoned plantations, and agroforestry plots (Menalled et al., 1998). Elevation ranges from approximately 35 to 135 m above sea level, with a north–south gradient resulting in higher elevations and steeper slopes to the south where the reserve borders on the Braulio Carrillo National Park. The soils at La Selva are primarily a mixture of inceptisols (particularly in alluvial terraces) in the north and residual ultisols to the south (Clark et al., 1998). These variations in soil and topography do not have a major impact on the magnitude of forest aboveground biomass, although they do impact stem size, density, stand dynamics, wood density, and the spatial heterogeneity of biomass (Baker et al., 2004; Chave et al., 2005; Clark & Clark, 2000; Saatchi & Moghaddam, 2000). Because of the variety of land cover types and the wealth of ancillary data (e.g., soil, topography, forest structure) available, La Selva is an excellent site for assessing variation in forest biomass over a variety of land use history types.

2.2. Field data

We acquired five different sets of inventory data (Table 1), covering variations of forest structure ranging from abandoned pasture to old-growth wet forests within and surrounding the La Selva Biological Stations (Fig. 1).

Carbono Plots: This set included 18 0.5 ha plots (each 50 m × 100 m) that were part of the landscape-scale study of carbon storage and flux in old-growth forests (Carbono project) (Clark & Clark, 2000). The inventory data were collected for woody stems ≥ 10 cm DBH (diameter at breast height) above buttresses. Aboveground biomass (AGB) was computed by using tropical wet forest allometric equation developed by Brown (1997).

$$AGB(\mathrm{kg}) = 21.297 - 6.95DBH + 0.740DBH^2 \quad (1)$$

BOSQUES plots: We acquired data from four 1 ha plots from the BOSQUES project focused on studying the dynamics of regeneration in wet tropical secondary forests (Chazdon et al., 2005).

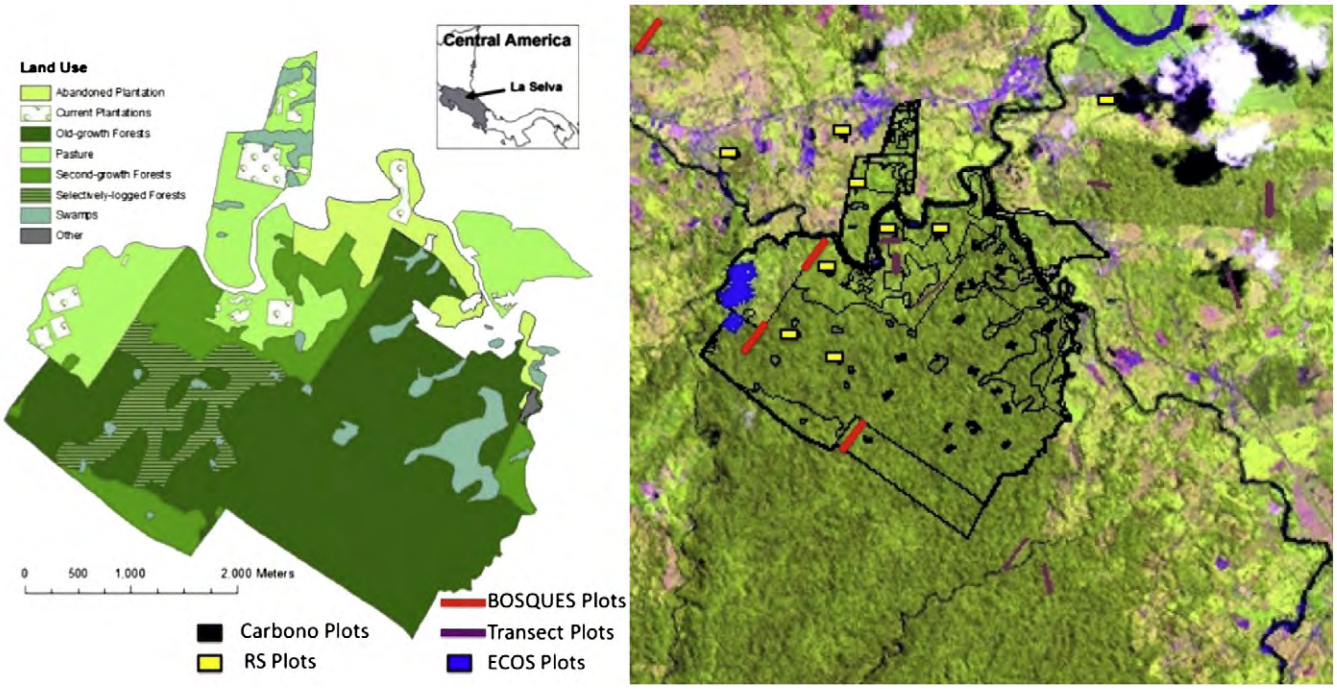

Fig. 1. Land use patterns and approximate location of sample plots with and surrounding the La Selva Biological Station overlaid on Landsat ETM imagery.

Table 1
List of forest inventory plots within and surrounding La Selva Biological Station, Costa Rica.

Plot name	Source	No. plots	Size ha	Vegetation type	Basal area range $M^2\ ha^{-1}$	AGB range $Mg\ ha^{-1}$
Carbono	D. Clark	18	0.5	Old growth forest	18–29	124–200
Transects	S. Saatchi	6	1.0	Old secondary and primary forests	20–31	44–516
		2	0.5			
BOSQUES	R. Chazdon	4	1.0	Secondary forest age 16–30	17–30	132–198
Peje Annex	A. Russell	40	0.25	Mixed tree plantations	9–51	36–237
AIRSAR campaign plots	S. Saatchi	8	1.0	Fallow and young secondary forests (age 1–12)	11–14	7–73

Inventory data included diameter of all trees ≥ 5 cm DBH and AGB using allometric Eq. (1). The field data was acquired in 2004, the same year the remote sensing data was acquired.

Remote Sensing Plots: We gathered data over 8 other 1.0 ha plots in areas dominated by low biomass forests (two abandoned pasture, one young secondary forest less than 10 year old, one young fallow, two secondary forests about 10 year old and two agroforestry sites). These plots represented biomass values ranging from less than10 $Mg\ ha^{-1}$ to less than 200 $Mg\ ha^{-1}$. Inventory of forest plots included trees ≥ 5 cm DBH. Forest AGB values were computed using Eq. (1). For pasture plots, woody biomass of trees was computed using the same approach.

Transect plots: This data set was collected during 2007 field campaign and included 6 1.0 ha (20 m × 500 m) and 2 0.5 ha (20 m × 250 m) transect plots in old-growth and old secondary forests (>20 years) within and surrounding the La Selva station. In all transects, we measured DBH (diameter at breast height) of all trees ≥ 10 cm diameter above buttresses, height of trees with visible crowns using inclinometer and laser range finder, and gap density using the fish-eye digital photography. We divided the transects into smaller 0.25 ha plots (20 × 125 m) to increase the number of points used in remote sensing data analysis and to capture the small scale variability in forest structure. We refer to these plots as transect plots. Tree diameters from these transects were transformed into AGB using the allometric Eq. (1).

ECOS Plots: The third data sets came from ECOS Project (Tree Species Effects on Ecosystem Processes: http://www.nrem.iastate.edu/ECOS/index.html) that included 40 0.25 ha (50 m × 50 m) plots out of 60 plots established in the Peje Annex of La Selva on a degraded landscape with tree plantations (Russell et al., 2007). The study area was cleared in 1955 by burning the slash and was under pasture and grazing until 1987. The experimental plantation was established in 1988 to study the impact of 11 native tree species on the soil properties. The inventory data included the tree density, diameter, height, and AGB. For these sites, species based allometric equations were used to estimate AGB for 0.25 ha plots.

We combined all the plots to develop a new set of plots at 0.25, 0.5, and 1.0-ha sizes for the multi-scale analysis of remote sensing data. We compiled 92 0.25-ha plots by breaking the 0.5 and 1.0-ha plots into 2 and 4 0.25-ha plots respectively. Similarly, we regrouped smaller plots to create a total of 49 0.5-ha plots and 28 plots of 1.0-ha in size. In the process, we assumed the 0.5-ha Carbono plots located within the old-growth forests of La Selva could be combined to represent 1.0-ha plot biomass values. This assumption was justified after performing the analysis for the spatial variability of forest AGB and was primarily used to allow us to combine pixels from remote sensing data to represent the average biomass of 1.0-ha size plots.

The accuracy of AGB values estimated from field measurements could not be assessed due to lack of destructive sampling of trees within the study area and the use of allometric equations developed elsewhere. However, some factors relating to the AGB accuracy were evaluated. Data from small (0.04 ha) sampling plots within the 1.0 ha transects showed that trees with 5 cm < DBH < 10 cm contributed approximately 5–10% of AGB, with higher numbers associated with secondary-growth forests. The contribution of trees less than 5 cm in DBH could be approximately the same (Montgomery & Chazdon, 2001). Other studies have shown that errors from allometric equations in tropical forests can range from ±10% to ±25% (Brown 1997; Chave et al., 2005). Knowledge of species level allometry, wood density, tree height, and the size of sampling plots will improve the accuracy of AGB. In this study, we expect that the AGB values associated with plots at various scales may have uncertainties varying from ±5% to ±20% from young secondary-growth to old-growth forests.

2.3. Remote sensing data

In March of 2004, the NASA/JPL (Jet Propulsion Laboratory) airborne SAR system, AIRSAR on the NASA DC-8 aircraft acquired polarimetric images along with simultaneous interferometric TOPSAR data over La Selva Biological Station. The entire La Selva was covered in various modes by changing the altitude, baseline, and repeat time in order to develop a baseline dataset to explore the application of polarimetric and InSAR techniques in tropical forests. The AIRSAR was operating at P-band (435 MHz, 20 MHz bandwidth), L-band (1.25 GHz, 40 MHz bandwidth) in fully polarimetric modes and C-band (5.3 GHz, 40 MHz bandwidth) at vertical polarization (VV) and interferometric mode. The polarized backscatter values derived from these measurements are HH, HV, and VV at both L-band and P-band frequencies, with H and V representing the horizontal and vertical transmit and receive polarizations. Data sets used in this study are acquired in 5 m spatial resolution at L-band and C-band and 10 m resolution at P-band, over a 12 km wide swath with incidence angles ranging from about 20 to 60° with approximately 45° at the center of the swath. All images were terrain corrected using the digital elevation data acquired by the TOPSAR interferometric modes and ground control points (Fig. 2). The images were also orthorectified in a Universal Transverse Mercator (UTM) projection using the available Quickbird data with a large number of ground control points that provided registration accuracy of approximately 15 m (1.5 pixels). The radar images were kept at 10 m resolution for further data analysis.

In addition to radar data, we had access to DEM (Digital Elevation Model) derived from lidar data acquired by the airborne Laser Vegetation Imaging Sensor in 2005. LVIS is a medium-altitude, medium- to large footprint imaging laser altimeter, designed and developed at NASA's Goddard Space Flight Center. LVIS digitizes the entire return signal, thus, providing a waveform relating to the vertical distribution of intercepted canopy and ground surfaces within each footprint (Blair et al., 1999; Dubayah & Drake, 2000). From LVIS data, we used the ground elevation (DEM) and canopy height metrics posted at 20 m grid cell over the La Selva. The DEM was measured as elevation above sea level and had an absolute accuracy of 3.37 m (http://www.ots.ac.cr/). The gridded LVIS DEM and the radar images

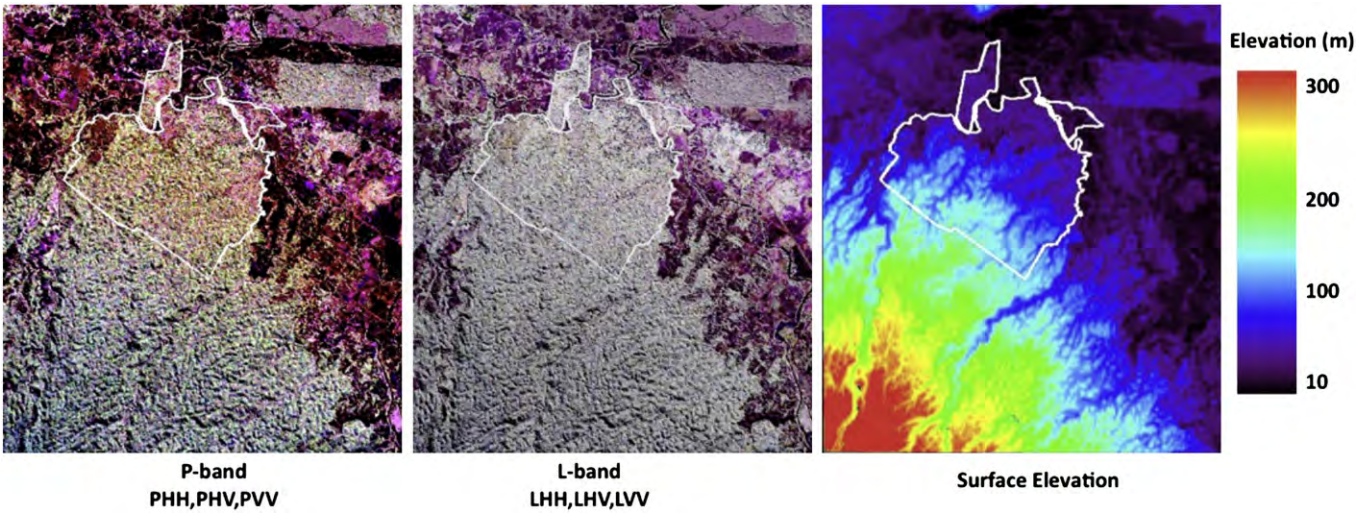

Fig. 2. AIRSAR polarimetric radar imagery and InSAR measured surface elevation acquired over the La Selva region in March 2004. The P-band and L-band images are false color composites with HH as red, HV as green, and VV as blue channels.

were co-registered to an accuracy of less than 1 pixel. The height metrics were RH100 and RH50. RH100 is the height of the first lidar return from the canopy minus the ground return, representing the maximum height of the forest canopy within the lidar footprint. RH50 is the 50% quantile metric, which represents the height below which 50% of the waveform energy is located (Drake et al., 2002).

3. Methods

3.1. Spatial variation of forest biomass

We analyzed the ground data using three different methods to understand and quantify the spatial variations of AGB. First, we analyzed the distribution of AGB in plots ranging from 0.01-ha to 1.0-ha by sub-dividing transect and RS plots over mature forests and old secondary forests. Second, we analyzed the variations of AGB within the plots by using the coefficient of variation of plot AGB. The analyses were performed in a completely nested approach, so that all the tree data used in 0.01 ha analyses are included in every analysis for larger plot sizes (Clark & Clark, 2000). Third, we used variograms to test for spatial autocorrelation in the AGB data. Variograms are a geostatistical technique to detect spatial autocorrelation between samples of a quantitative variable (e.g. AGB) (Isaaks & Srivastava, 1989). In a variogram, the averaged squared difference in the value of a variable between all pairs of plots is computed across distance intervals (lag classes). The output is often presented as a variogram plot of the average semivariance versus distance classes. The semivariance converges at a distance for which values are no longer spatially autocorrelated and are spatially independent. Three parameters estimated from the variogram model quantify the scale of spatial dependence: the nugget refers to y intercept and represents either the microscale variations or measurement errors. The sill refers to maximum value of semivariance signifying the total variance in the data. The range refers to the distance at which the semivariance reaches 95% of the sill. These parameters are estimated from spherical models that are fitted to the empirical variograms using a non-linear least squares method (Isaaks & Srivastava, 1989). All spatial statistics were computed using GS+ software (Gamma Design Software, Plainwell, Michigan). The empirical variograms were calculated using AGB of 0.01-ha subplots from all Carbono and transect plots and with a lag distance of 10 m.

3.2. Sensitivity of radar backscatter to AGB

To assess the accuracy of AGB estimation from radar measurements, we examined the overall sensitivity of the radar backscatter to AGB and quantified the errors associated with the estimation algorithm. We investigated the impact of the spatial variation of the forest structure and errors associated with the geolocation of the plots, measurement geometry, and the speckle noise. In general, at low frequencies (e.g. L-band and P-band) the radar transmitted energy, in the form of an electromagnetic pulse, penetrates into the forest canopy and reflects back from forest components such as leaves, branches, stems, and underlying soil. Knowing the magnitude of transmitted and received energy, a physical relationship, based on electromagnetic theory, has been developed to relate the ratio of these energies to properties of the forest. The measurements are performed in a combination of transmit and receive polarizations (H: Horizontal, and V: Vertical), at an off-nadir incidence angle, and at a spatial resolution projected on the radar range direction. Therefore, radar backscatter measurement at any frequency and polarization combinations (e.g. HH, HV, VV) depends on two sets of parameters: 1. Measurement geometry such as incidence angle and location and size of the image pixels with respect to the size and the orientation of plots. 2. Forest structural parameters such as the size (volume) and density (number per resolution cell) of trees, orientation of the forest components (leaves, branches, stems), underlying surface condition (moisture, roughness, and slope), and the dielectric constant that in turn depends on the vegetation water content or specific gravity (i.e. the wood density). Dependence on these variables makes radar measurements sensitive to forest AGB (Dobson et al., 1995; Saatchi & Moghaddam, 2000).

Depending on the wavelength of the measurement, the radar backscatter from a forest can be related to scattering from live stems, branches, and foliage based upon their abundance and moisture content within a resolution cell as:

$$\sigma^0_{pq} \propto f_{pq}(\eta_i, V_i, \varepsilon_i) \tag{2}$$

Where f_{pq} is a function averaged over all possible orientation and size distributions, and p and q represent the transmit and received polarizations. The forest components (stems, branches, leaves) within a unit area of the radar image pixel are represented by density of trees η_i, volume V_i, and dielectric constant ε_i. Eq. (2) symbolically

represents the radar backscatter relationship to forest structure and wood density that, along with orientation and tree size distributions, can be used to generate a model for estimating forest volume or biomass.

In forestry applications, this model is simplified to a parametric or regression type relationship designed to directly estimate the AGB. To examine the sensitivity of radar backscatter measurements to AGB, first, we calculate the value of backscattering coefficient at each polarization normalized for incidence angle by normalizing the pixel value with the cos (θ_0) (Ulaby et al., 1982). The normalized value of backscattering coefficient is shown by γ_{pq}, where p and q are either H or V and represent the received and transmitted polarizations respectively. This value is often represented in logarithmic scale in decibels (dB), but here it has been transformed to linear scale in $m^2\ m^{-2}$ for simplicity of data analysis. We examine the value of backscattering coefficients in terms of AGB at L-band and P-band frequencies at various spatial scales.

3.3. Estimation of AGB from radar backscatter

Estimation of AGB from radar backscatter was performed by using a statistical regression model between AGB and the radar backscatter at different polarizations. Based on previous studies, the regression model was developed between an unknown power of AGB and a linear combination of backscatter measurements at three polarizations (Ranson & Sun, 1994; Saatchi et al., 2007):

$$AGB^{\lambda} = a_0 + a_1\gamma_{HH} + a_2\gamma_{VV} + a_3\gamma_{HV} \quad (3)$$

Where the unknown coefficients (λ, a_0, a_1, a_2, and a_3) will be determined statistically by using radar measurements and field data at three spatial scales of 0.25, 0.5, and 1.0 ha. The analysis also included the use of single polarization or dual-polarization radar data in order to simulate the accuracy of AGB when only one or two channels are available in future spaceborne radar data at L-band and P-band. The overall form of the regression model used in this study may not be ideal when used for all combinations of frequency and polarizations. However, it will provide us with a simple algorithm to test the performance of radar measurements. In the regression model, we also assume that the backscatter coefficients are normalized by incidence angle and have been projected on the ground using available surface topography over La Selva. In an ideal case, where there are large variations in surface topography, a more complex algorithm can be developed that includes the impact of surface slope on scattering mechanism of radar signal within the forest (Saatchi et al., 2007).

3.4. Forest height index from InSAR measurements

In addition to the polarimetric backscatter measurements, we also make use of the elevation measured by Interferometric SAR (InSAR) measurements at C-band and VV polarization to estimate the vegetation height. Over vegetated surfaces, the InSAR measures a height below the vegetation canopy known as the height of scattering phase center. This height is given by (Zebker & Villasenor, 1992):

$$h_s + h_{sc} = H - \rho\ cos\,(\alpha - \theta) \quad (4)$$

$$h_{sc} = H - h_s - \rho\ cos\left(\alpha - sin^{-1}\left(\frac{\lambda\Delta\phi}{4\pi B}\right)\right)$$

Where h_s and h_{sc} are the surface (bald earth) elevation and the height of the scattering center respectively. The radar platform is located at an altitude of H, the InSAR baseline distance is given by B, and the angle by α. The phase difference measured by the radar is given by $\Delta\phi$ and the range distance to the center of the pixel is approximately given by ρ. In Eq. (4) all parameters are given except h_s and h_{sc}. For the surface elevation, we use the digital elevation data provided by the lidar measurements of underlying forest surface acquired in 2005. Once h_{sc} is derived from Eq. (4), it can be used directly in the regression model to improve the estimation of AGB. The value h_{sc} represents the average forest height weighted by the canopy density or the basal area (Sarabandi & Lin, 2000). That is, for forests of open canopy or relatively low basal area, h_{sc} is smaller than for forests with dense canopy cover. We refer to h_{sc} as the height index throughout the paper and examine its contribution to improve the biomass estimation using the following relationship:

$$AGB^{\lambda} = a_0 + a_1\gamma_{HH} + a_2\gamma_{VV} + a_3\gamma_{HV} + a_4 h_{sc} \quad (5)$$

Where the linear dependence on the height index is justified from recently developed relationships between average or basal area weighted heights and the aboveground biomass (Drake et al., 2002; Lefsky et al., 2005).

4. Results

4.1. Spatial variability in biomass

There are various uncertainties in estimating the AGB of a sample plot. Under the assumption that the allometric models are perfect and the tree-level uncertainties average out at the stand level, a typical error of 10% of the mean for AGB estimates can be encountered for plot sizes of one-quarter of a hectare (0.25-ha) (Chave et al., 2003). Spatial variability of forest structure, large effects of individual trees with large DBH, lack of sampling of small trees (DBH<5 cm), and errors in measuring DBH of trees in the field (trees with buttresses) are the main sources of errors in estimating the biomass of a forest stand.

First, we analyzed the distribution of AGB in old-growth forests for sub-plots of varying sizes and tested for normality of the data (Fig. 3). This analysis showed that at smaller sub-plots, the AGB distribution was skewed to the left and had a large range from 0 to 1342 and 20 to 542 Mg ha^{-1} for of 0.01-ha (10 m × 10 m) and 0.04 ha (20 m × 20 m) sub-plots respectively. For larger sub-plots (0.25–1.0 ha) we combined the Carbono plots and transects to create the histograms. The results suggested that 0.25-ha (50 m × 50 m) is the minimal size required for a normal distribution of biomass. An indicator for the normality was the symmetric probability distribution and small skewness and kurtosis. The Shapiro–Wilk normality test was performed on the distributions and it was shown that for plots greater than or equal 0.25 ha, the distributions passed the test ($p>0.05$).

We combined transect and Carbono plots to examine variations in AGB with plot size in terms of the coefficient of variations (CV) (Fig. 4). As the plot size increased, CV continued to decrease to approximately 10% at the 1.0 ha plot size. At smaller plots, the possibility of occurrence of a large tree can create heterogeneity in forest structure and large variations in biomass. These variations are averaged out at lager plot sizes. The CV values at 1.0 ha scale were computed by using the 1.0 ha transect plots in old-growth forests and by combining 18 0.5 ha Carbono plots to virtually generate 9 1.0 ha plots. As the Carbono plots are separated from each other and have no spatial correlations, we expect the CV values represent the upper bound to the coefficient of variations at 1.0 ha scale because contiguous 1.0 ha plots have less variations.

To assess the scale of spatial dependence, we analyzed semivariograms of forest biomass for 18 Carbono plots and 8 transects. Spherical models with lag distances of 5 to 100 m provided excellent fits to all stands with average R^2 of 0.93. In all cases, the forest biomass showed very high spatial variability with average range of about 11 m, suggesting neighboring sub-plots from 0.01 ha in size to 1.0 ha are statistically independent. In other words, the AGB in sub-plots in forest stands is not significantly autocorrelated at a scale larger than

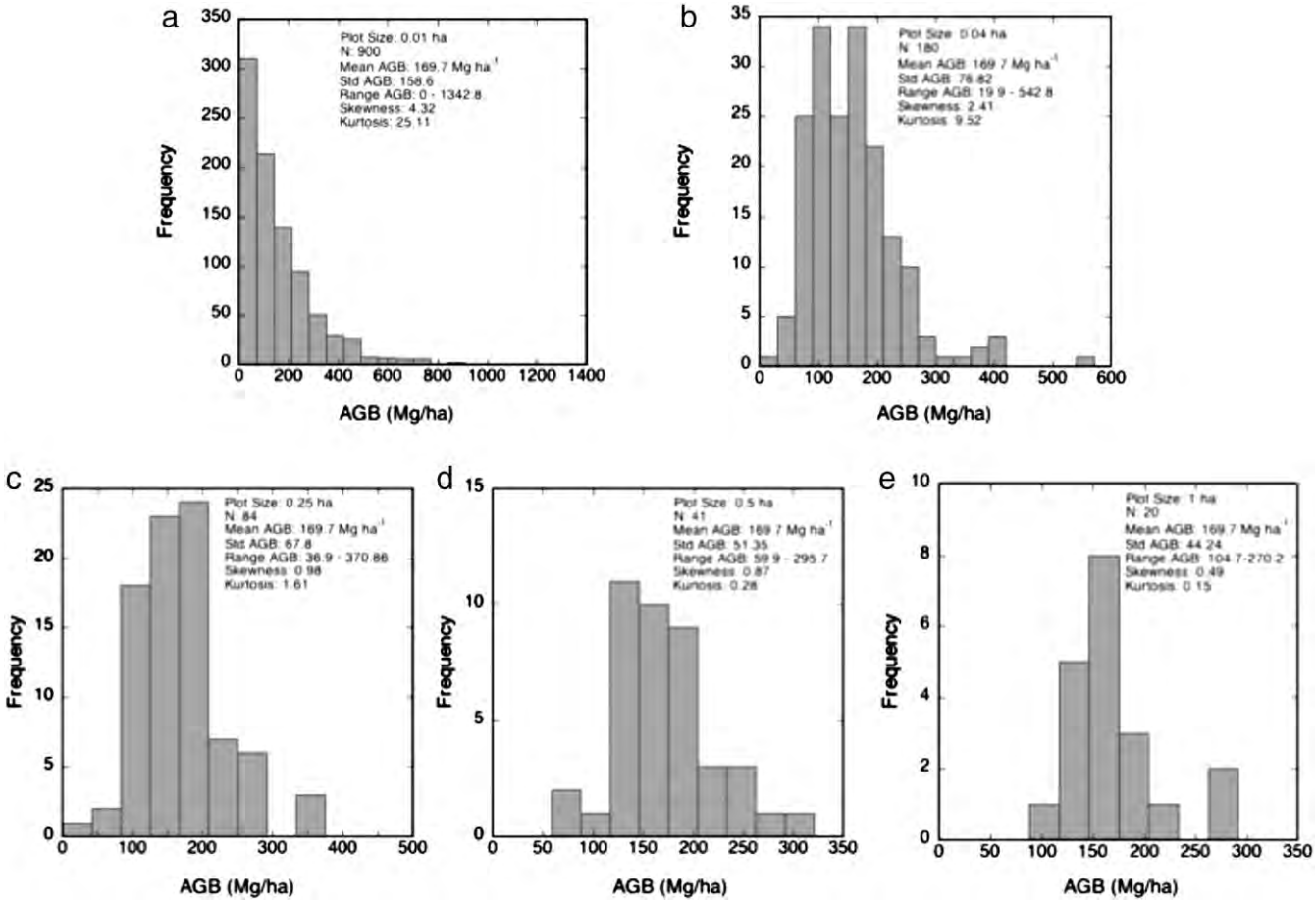

Fig. 3. Distribution of forest biomass over the old-growth forests sampled at different plot size using the Carbono and transect plots: (a) 0.01 ha plot size, (b) 0.04 plot size, (c) 0.25 ha plot size, (d) 0.5 ha plot size, and (e) 1.0 ha plot size.

11 m. The semivariogram analysis for La Selva plots confirmed the results obtained in the 50-ha plot of Barro Colorado Island in Panama (Chave et al., 2003). A similar independent study, using Carbono plots in La Selva showed autocorrelations in forest biomass dropped to insignificant at distances larger than 11 m (David Clark, Personal Communication). This analysis will not provide any significant information about the variability of the forest biomass at scales larger than 1.0 ha.

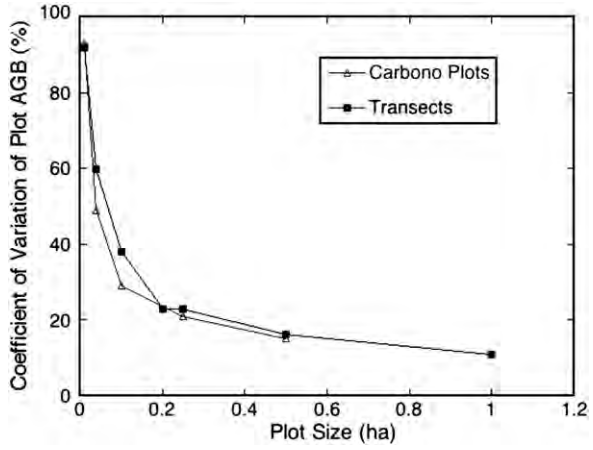

Fig. 4. Coefficient of variation of ground-estimated aboveground biomass in relation to plot size for old-growth forests of Carbono and transect plots.

4.2. Radar backscatter sensitivity to biomass

Normalized backscatter coefficients at HH, HV, and VV polarizations were extracted from 10 m pixel resolutions for plot sizes at 0.25, 0.5, and 1.0 ha. The results for L-band and P-band frequencies are shown in Figs. 5 and 6. A power–law relationship was the optimum fit to the normalized backscatter data with respect to the aboveground dry biomass in all cases. At both frequencies, the scale of analysis did influence the relationship between AGB and backscatter. As the scale of analysis increased from 0.25 ha to 1.0 ha, the r-squared correlation between backscatter and AGB improved, largely due to the spatial averaging of the radar data and the reduction of speckle noise. The improvement from 0.25 to 0.5 ha was due to both reduction in the speckle noise and the errors due to geolocation and orientation of the plots. Whereas, the improvement from 0.5 to 1.0 ha plots was mostly due to averaging a larger number of pixels and hence the reduction of speckle noise. Although all polarizations showed similar trends with respect to increasing AGB, there were clear distinctions among them in terms of backscatter level and sensitivity to biomass. In both frequencies, the HV sensitivity to biomass was much higher and the relationship improved much higher than other channels as the scale of measurement increased. However, at L-band the sensitivity to biomass decreased rapidly at 100 Mg ha^{-1} at 0.25 ha and with slightly higher value of 100–150 Mg ha^{-1} at the 1.0 ha scale.

The P-band results showed a very strong relationship to AGB over the entire range, with gradual loss of sensitivity at AGB>200 Mg ha^{-1}. The r-squared correlation between P-band channels and AGB was almost above 0.7 in all cases and improved with increases in spatial scale.

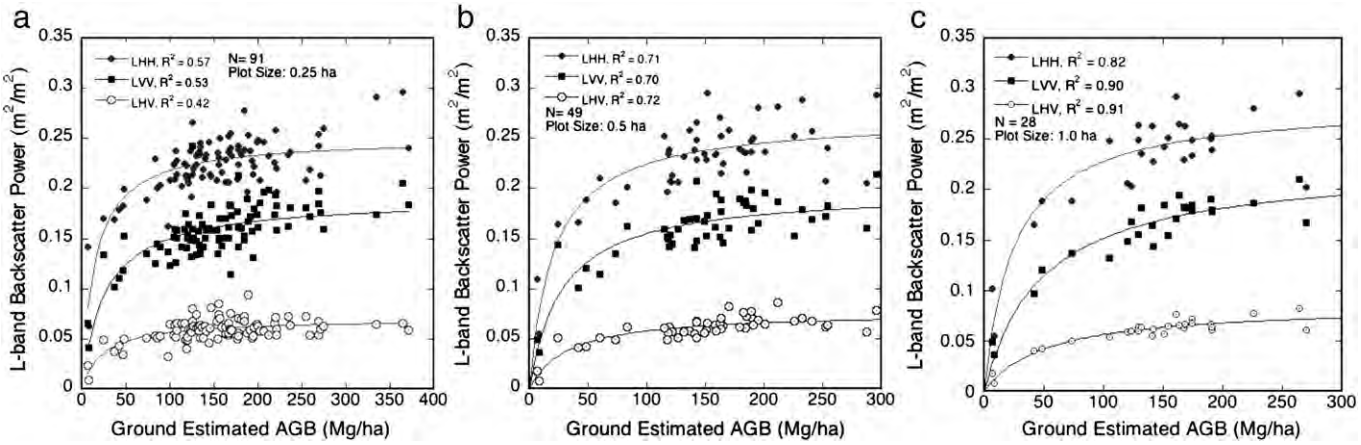

Fig. 5. Relationship of L-band radar backscatter power ($m^2\ m^{-2}$) at three polarizations of HH, HV, and VV with the aboveground biomass (Mg ha^{-1}) and at three scales: (a) 0.25 ha, (b) 0.5 ha, and (c) 1.0 ha.

To further examine the sensitivity at 1.0 ha spatial resolution, we calculated the differences in backscatter power for every 50 Mg ha^{-1} and transformed the power in dB values for radar calibration purposes. The dynamic range from low to high biomass values averaged over all polarizations was approximately 7.0 dB for L-band and 11 dB for P-band, with the largest portion of dynamic range for the AGB<0–100 Mg ha^{-1}. At the L-band frequency, the biomass values above 100 Mg ha^{-1} covered less than 2 dB of backscatter power, whereas, at P-band this range was about 4.5 dB (Table 3).

Given the overall sensitivity of backscatter power to AGB, we used Eqs. (3) and (4) to develop regression models to estimate AGB for a combination of polarized backscatter at L-band and P-band frequencies. The first step in the regression analysis was to estimate λ, the power of the AGB. This step was done using the REGRESS routine in IDL to perform a multi-variable linear regression analysis. The estimated values of λ for models including dual or all polarizations at L-band and P-band ranged between 0.34 and 0.58. In order to obtain a single value of λ for all cases, we simulated equations with λ values ranging from 0.34 to 0.58 for all model runs, and calculated the residual errors in biomass estimation between optimum and simulated λ for all models and choose the λ with the least residual error. In all cases, the best relationship was found for λ = 0.47. We set λ = 1/2 for all regression models for simplicity and comparability of models. The regression models were performed for the single-polarization dual-polarization with (HH, HV), and the quad-polarization with HH, HV, VV (HV = VH in all measurements) backscatter power.

4.3. L-band estimation of biomass

Estimation of AGB from L-band measurements was performed for single and multiple polarized backscatter at three spatial scales and results are summarized in Table 2. The root-mean-squared errors (RMSE) for the entire range were calculated by using two methods: 1. The leave-one-out cross-validation approach where the RMSE error is estimated by calculating the errors associated with an algorithm developed from all sample points except one. 2. The hold-out approach where the generalization error is estimated by retaining a subset of sample points (20%) as validation set. For RMSE of biomass values less than 200 and 100 Mg ha^{-1} we only used the leave-one-out approach because of the limited sample size.

Errors associated with single polarization measurements were approximately the same for HH and HV across the scales with the exception of 1.0 ha plots where biomass estimation improved for LHV especially for AGB < 100 Mg ha^{-1}. For all scales, the error associated with the single polarization algorithm was larger than 20% of the mean biomass. The error reduced to approximately 10–15% for dual polarization

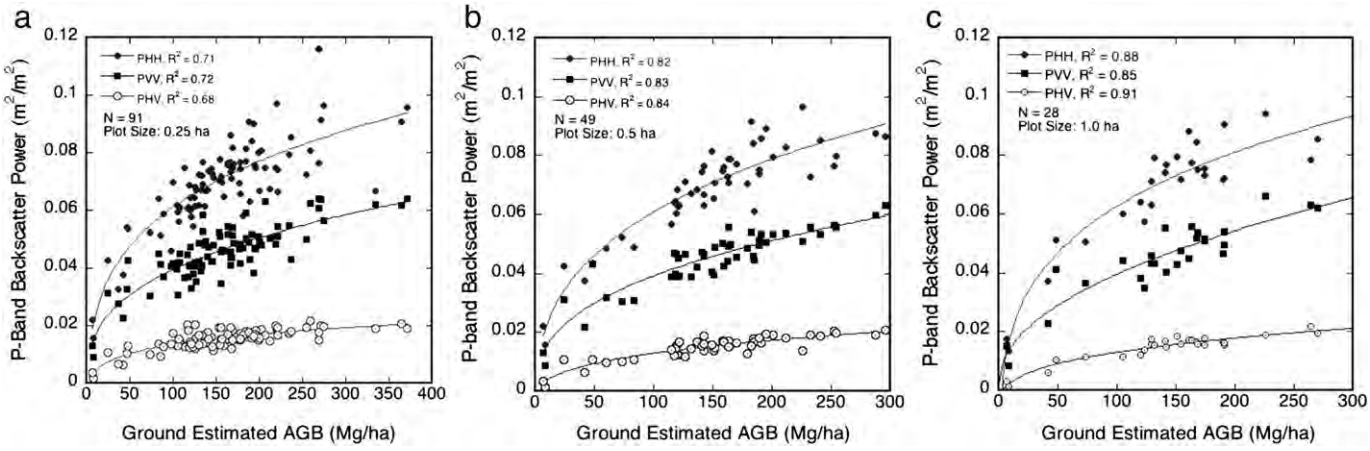

Fig. 6. Relationship of P-band radar backscatter power ($m^2\ m^{-2}$) at three polarizations of HH, HV, and VV with the aboveground biomass (Mg ha^{-1}) and at three scales: (a) 0.25 ha, (b) 0.5 ha, and (c) 1.0 ha.

Table 2
Radar backscatter dynamic range and biomass estimation accuracy for a combination of L-band and P-band polarizations at three spatial scales of 0.25 ha, 0.5 ha, and 1.0 ha.

Radar channels	0.25 ha				
	AGB range: 7–370.9 Mg ha^{-1}				
	γ^0 range	R^2	RMSE all	RMSE (<200)	RMSE (<100)
			Mg ha^{-1}	Mg ha^{-1}	Mg ha^{-1}
LHH	−12.6, −4.8	0.42	51.6 (56.1)	43.9	42.3
LHV	−20.9, −10.2	0.39	53.4 (58.2)	36.8	43.9
LVV	−14.4, −5.7	0.27	62.8 (68.9)	44.5	54.4
PHH	−18.2, −8.9	0.58	44.0 (47.3)	27.6	30.5
PHV	−28.2, −16.4	0.67	38.8 (41.3)	34.8	38.6
PVV	−20.6, −11.5	0.53	46.3 (50.1)	37.3	38.4
LHH,LHV	NA	0.60	44.5 (49.6)	40.2	30.1
LHH,LHV,LVV	NA	0.62	42.5 (48.2)	37.7	26.8
PHH,PHV	NA	0.74	32.6 (35.3)	27.5	28.5
PHH,PHV,PVV	NA	0.79	30.7 (34.1)	24.3	27.9
Radar channels	0.5 ha				
	AGB range: 8–295.7 Mg ha^{-1}				
	γ^0 range	R^2	RMSE all	RMSE (<200)	RMSE (<100)
			Mg ha^{-1}	Mg ha^{-1}	Mg ha^{-1}
LHH	−12.6, −5.3	0.54	48.3 (53.1)	42.3	33.9
LHV	−20.9, −10.7	0.58	44.5 (49.5)	38.6	32.1
LVV	−14.4, −6.7	0.53	46.1 (50.2)	42.4	34.3
PHH	−18.2, −9.7	0.67	43.3 (45.0)	30.34	34.1
PHV	−28.2, −16.6	0.67	37.2 (39.1)	26.5	31.2
PVV	−20.6, −11.9	0.65	38.5 (42.3)	35.9	35.4
LHH,LHV	NA	0.58	43.5 (48.2)	37.9	35.1
LHH,LHV,LVV	NA	0.62	39.5 (43.2)	34.3	34.3
PHH,PHV	NA	0.80	28.6 (30.5)	24.9	24.8
PHH,PHV,PVV	NA	0.83	26.6 (28.3)	23.8	21.5
Radar channels	1.0 ha				
	AGB range: 8.1–270.1 Mg ha^{-1}				
	γ^0 range	R^2	RMSE all	RMSE (<200)	RMSE (<100)
			Mg ha^{-1}	Mg ha^{-1}	Mg ha^{-1}
LHH	−12.6, −5.3	0.67	39.6 (41.4)	29.4	23.1
LHV	−20.9, −10.8	0.66	34.6 (37.7)	23.1	14.1
LVV	−14.4, −6.7	0.68	38.1 (42.8)	28.7	19.8
PHH	−18.2, −10.2	0.77	31.8 (34.5)	24.6	14.8
PHV	−28.2, −16.6	0.86	24.6 (27.4)	23.5	12.5
PVV	−20.6, −11.8	0.83	27.6 (33.3)	27.2	26.7
LHH,LHV	NA	0.73	35.1 (40.2)	31.7	15.7
LHH,LHV,LVV	NA	0.75	33.1 (37.1)	28.3	13.8
PHH,PHV	NA	0.88	22.6 (24.3)	20.5	17.0
PHH,PHV,PVV	NA	0.91	19.9 (22.2)	18.6	15.3

(RMSE = 15.7 Mg ha^{-1}) and all polarizations (RMSE = 13.8 Mg ha^{-1}) for AGB < 100 Mg ha^{-1} range. Over the entire biomass range, the estimation accuracy improved when moving from 0.25 ha to 1.0 ha (Fig. 7). However, the statistics of the plot-by-plot difference between the predicted and ground estimated biomass showed a bias towards lower values, suggesting the L-band loss of sensitivity to predict biomass values above a certain threshold (Fig. 8). By focusing at AGB < 100 Mg ha^{-1}, the estimation bias disappears and the error becomes approximately normally distributed for all scales greater or equal to 0.25 ha. The biomass threshold may be higher than 100 Mg ha^{-1}, especially at 1.0 ha scale, if larger errors are tolerated. However, because of the small dynamic range of backscatter power (approximately 2 dB for AGB > 100 Mg ha^{-1}), and the errors associated with the multiple polarization algorithms, L-band algorithms may not provide reasonable estimates for biomass values above 100 Mg ha^{-1}.

4.4. P-band estimation of biomass

The P-band based algorithms out-performed L-band's across biomass ranges and spatial scales. Errors associated with single polarized backscatter measurements were larger than 20% at 0.25 and 0.5 ha and reduced to between 10 and 20% at 1.0 ha scale. PHH and PHV performed better than PVV over the entire biomass ranges and scales. The accuracy of PHV estimation of biomass improved when the scale of the analysis increased from 0.25 to 1.0 ha. Combining the polarizations, either in dual (PHH, PHV) or multiple (PHH, PHV, PVV), reduced RMSE to approximately 10–15% over the entire range and at all spatial scales. Although P-band sensitivity to low biomass values (AGB < 20 Mg ha^{-1}) is often questionable because of the influence of soil moisture and surface roughness, at 1.0 ha spatial scale, the RMSE for AGB < 100 Mg ha^{-1} range was reasonably low at approximately 15 Mg ha^{-1}. The multiple polarization algorithm was capable of producing biomass estimates with less than 10% error for all three scales and over the entire range (Fig. 9). At 1.0 ha spatial scale, the RMSE from multiple polarization algorithm was bounded to 19–23 Mg ha^{-1} for leave-one-out method and 22–24 Mg ha^{-1} for hold-out approach. Statistics of the difference between predicted and ground estimated AGB showed almost no estimation bias and the errors were distributed almost normally at all scales (Fig. 10).

4.5. InSAR estimation of canopy height

The height index (h_{sc}) was estimated from InSAR measurements at C-band by subtracting the InSAR measured elevation from LVIS measured ground elevation. The height index was compared to average RH100 and RH50 measured by LVIS lidar over the Carbono,

Table 3
Estimated regression coefficients for above-ground biomass estimation from L-band and P-band multiple polarized backscatter and InSAR height index.

Radar channels	a0	a1	a2	a3	a4
0.25 ha scale					
LHH,LHV,LVV	−4.36	41.68 ± 2.56	45.71 ± 6.05	2.08 ± 2.53	–
LHH,LHV,LVV, h_{sc}	−4.31	35.51 ± 2.81	21.67 ± 6.25	−8.13 ± 2.79	0.36 ± 0.02
PHH,PHV,PVV	−1.23	64.11 ± 6.05	235.41 ± 22.80	119.41 ± 8.73	–
PHH,PHV,PVV, h_{sc}	−1.28	59.08 ± 6.26	155.12 ± 25.78	90.61 ± 9.61	0.19 ± 0.028
0.5 ha scale					
LHH,LHV,LVV	−1.91	16.49 ± 3.32	63.76 ± 11.28	39.26 ± 3.93	–
LHH,LHV,LVV, h_{sc}	−2.06	16.93 ± 3.65	56.87 ± 11.45	17.11 ± 4.26	0.26 ± 0.032
PHH,PHV,PVV	−0.31	57.96 ± 6.36	313.29 ± 30.79	81.22 ± 11.07	–
PHH,PHV,PVV, h_{sc}	−0.51	80.48 ± 10.28	176.39 ± 45.76	76.82 ± 18.18	0.05 ± 0.04
1.0 ha scale					
LHH,LHV,LVV	−0.67	−7.35 ± 4.87	106.63 ± 21.96	48.11 ± 6.72	–
LHH,LHV,LVV, h_{sc}	1.18	3.45 ± 4.02	4.95 ± 2.37	5.98 ± 5.67	0.57 ± 0.03
PHH,PHV,PVV	0.73	42.13 ± 13.49	323.02 ± 64.41	71.51 ± 18.74	–
PHH,PHV,PVV, h_{sc}	0.11	98.52 ± 17.89	184.1 ± 35.39	14.45 ± 8.06	0.083 ± 0.05

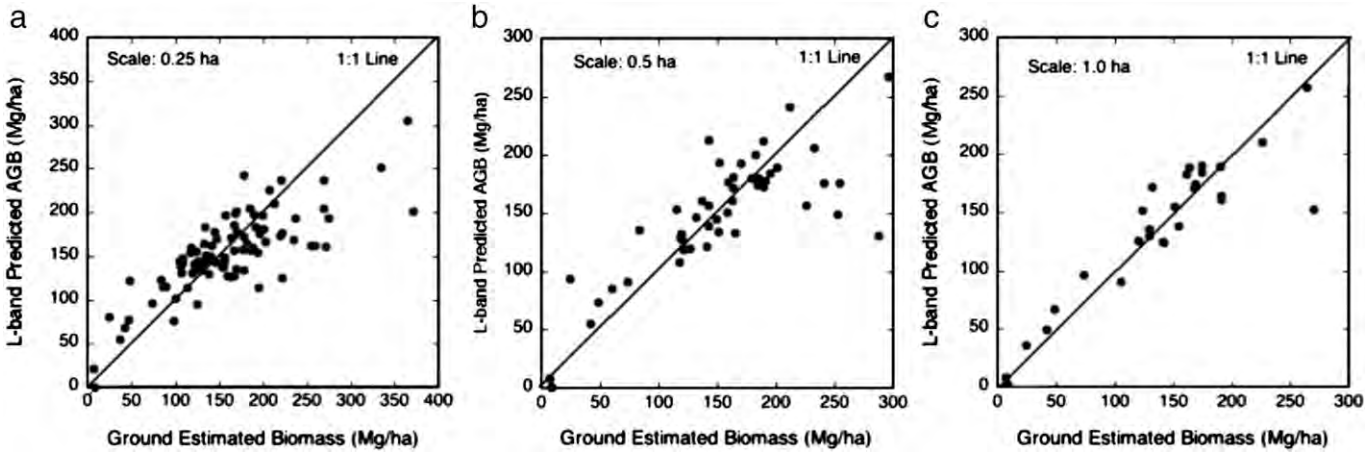

Fig. 7. Predicted vs. ground estimated aboveground biomass from L-band radar backscatter measurements with three polarizations of HH, HV, and VV and at three spatial scales: (a) 0.25 ha, (b) 0.5 ha, and (c) 1.0 ha.

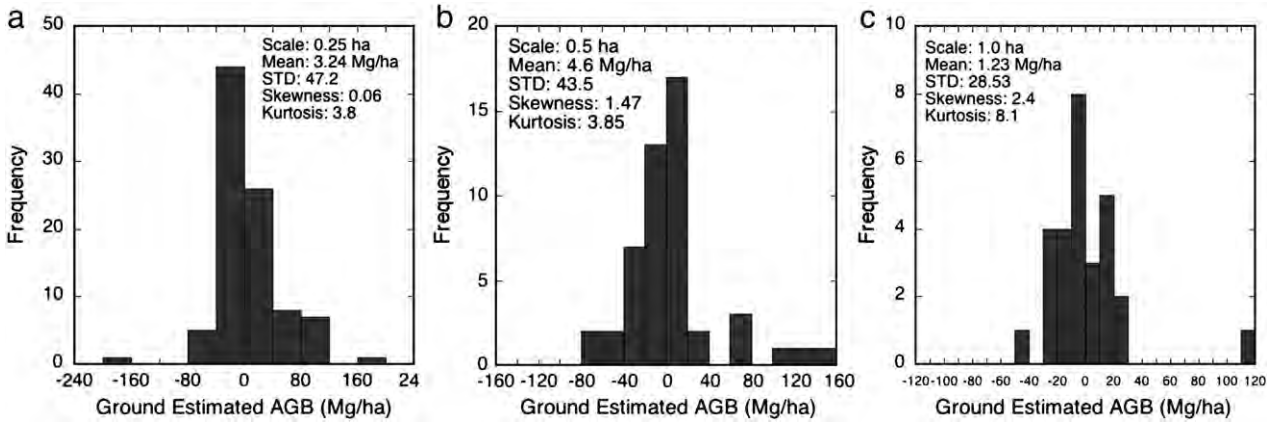

Fig. 8. Distribution of plot-by-plot estimation error (predicted−ground estimated) from L-band polarimetric algorithm using three polarizations of HH, HV, and VV, and at three spatial scales: (a) 0.25 ha, (b) 0.5 ha, and (c) 1.0 ha.

ECOS, and transect plots (Fig. 11). The height index had a significant correlation with both RH100 ($R^2 = 0.55$, $p < 0.001$) and RH50 ($R^2 = 0.62$, $p < 0.001$) averaged over all 20 m pixels within the plots. The average height metrics from LVIS and height index estimated over the transect plots contributed significantly to the dispersion of data points in Fig. 10c. The dispersion was mainly due to mixed pixel information caused by the narrow width and slanted shape of transects, introducing heights from neighboring pixels in average height estimation. The better correlation of the height index with RH50 was probably due to the impact of the forest structure (e.g. basal area, gap distribution, and canopy structure) on both metrics. Ideally, the relationships in Fig. 11c can be used to calibrate the height index to either RH100 or RH50. The RH100 values derived from InSAR and measured by LVIS are shown for comparison in Fig. 11a and b. Both

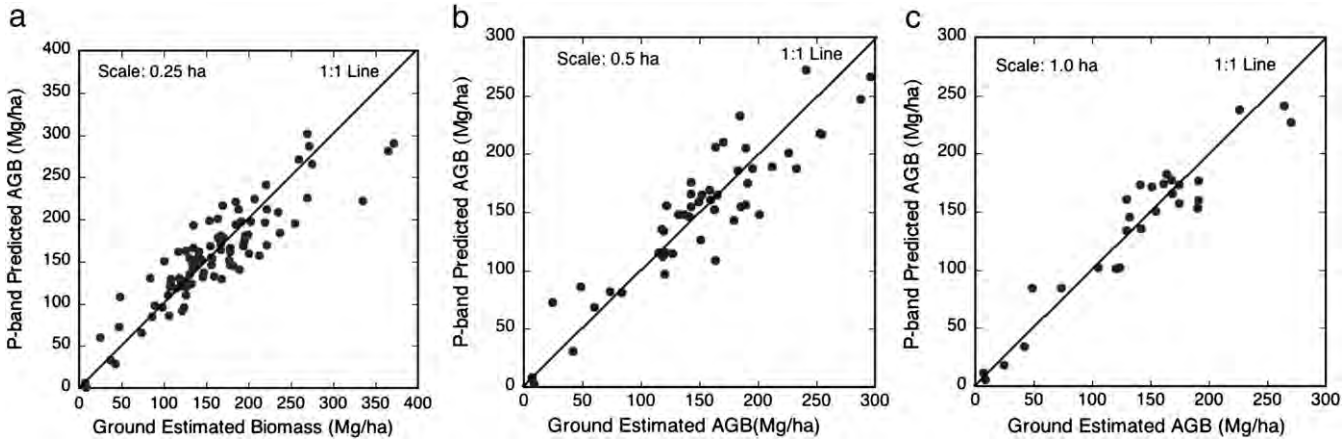

Fig. 9. Predicted vs. ground estimated aboveground biomass from P-band radar backscatter measurements with three polarizations of HH, HV, and VV and at three spatial scales: (a) 0.25 ha, (b) 0.5 ha, and (c) 1.0 ha.

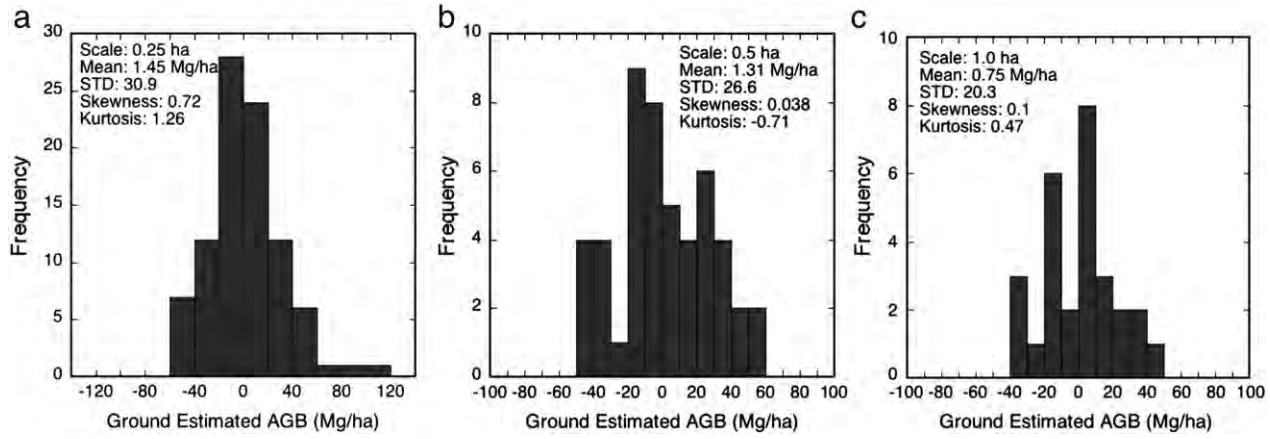

Fig. 10. Distribution of plot-by-plot estimation error (predicted − ground estimated) from P-band polarimetric algorithm using three polarizations of HH, HV, and VV, and at three spatial scales: (a) 0.25 ha, (b) 0.5 ha, and (c) 1.0 ha.

images show similar patterns of vegetation height over La Selva with the short secondary forests and plantations on the western side and the mature and tall forests on the eastern side of La Selva. The images also show that the InSAR-derived RH100 from the linear regression model overestimates height in the upper end of the height range and underestimates in the lower range. This suggests that the relationship between the InSAR estimated h_{sc} and RH100 might be non-linear and require further study to improve.

4.6. Biomass estimation from backscatter and InSAR height index

Eq. (4) was used to combine the height index with all polarized backscatter powers to estimate AGB. We performed the analysis at all three scales and for L-band (Fig. 12) and P-band (Fig. 13) with all polarizations. The contribution of the height index varied based on the scale of the analysis. At L-band, the addition of height improved RMSE by 18% at 0.25 ha, 22% at 0.5 ha, and 39% at 1.0 ha (Fig. 12). The changes of RMSE were primarily from improvements of estimation errors for AGB<200 Mg ha^{-1}. Higher biomass values improved slightly but remained underestimated at all scales.

The contribution of the height index to P-band backscatter estimation of biomass was as significant as in the L-band (Fig. 13). The RMSE improved by 7% at 0.25 ha, 24% at 0.5 ha, and 19% at 1.0 ha. However, the improvements were over the entire range, particularly for AGB>200 Mg ha^{-1}. In general, the addition of the height index had two significant effects on the biomass estimation from radar measurements: 1) It reduced the RMSE errors to approximately ±10% of the mean biomass at P-band and ±15% at L-band; and 2). It enhanced the range of the biomass estimation to slightly over 200 Mg ha^{-1} at L-band and over 300 Mg ha^{-1} at P-band. Using the height index alone to estimate AGB produced RMSE values similar to multi-polarized backscatter regression at L-band, but with better accuracies at higher biomass values (not shown here). The results suggested that the combination of backscatter power and the height index in estimation techniques would improve the biomass accuracy across the biomass range and the spatial scales. The coefficients in the estimation algorithm defined by Eqs. (2) and (3) for multiple polarization and height index are summarized in Table 3.

5. Discussion

We demonstrated that both L-band and P-band data are sensitive to the AGB of tropical forests and can be used to provide accurate estimates of biomass within a limited range. The extent of this range depends on the wavelength of the radar measurement, incidence angle, and the density of forest canopy that together control the radar

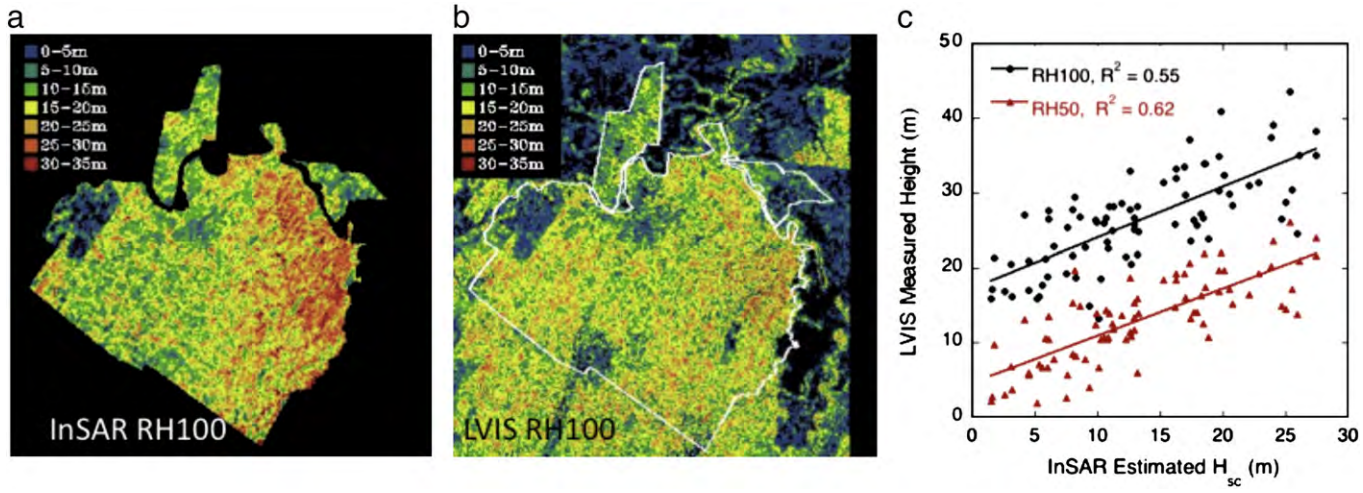

Fig. 11. Estimation of height index from InSAR measurements at C-band VV polarization: (a) InSAR derived height index (InSAR surface elevation−lidar derived ground elevation), (b) lidar derived vegetation maximum height RH100, (c) comparison of InSAR height index with lidar derived maximum height (RH100) and the height at the 50% energy level (RH50).

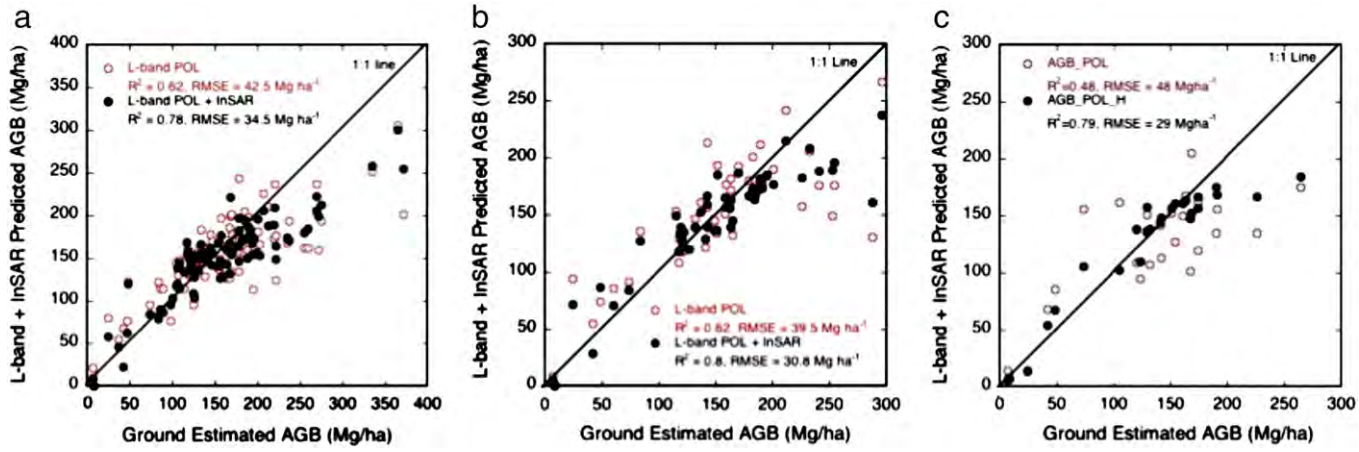

Fig. 12. Predicted vs. ground estimated aboveground biomass from L-band radar backscatter measurements at HH, HV, and VV polarizations and the InSAR derived height index at three spatial scales: a) 0.25 ha, (b) 0.5 ha, and (c) 1.0 ha.

signal penetration into the canopy and hence the magnitude of scattering from stems and branches. The accuracy of the estimation, however, depends on the spatial variability of forest structure and hence the spatial scale of the measurement, and other environmental variables such as moisture condition and phenology. In this study, we concentrated on the spatial variability of the forest structure and how it impacts the radar estimation of AGB.

5.1. Spatial scales

The analysis of spatial variability of forest structure and the biomass estimation from radar imagery would have been difficult to perform without access to a large number of forest inventory plots at different sizes. One of the key results of our research was the large variability of forest structure and biomass at small spatial scales. Semivariogram analysis of AGB showed almost no autocorrelation at lag distances above 11 m. Other studies in La Selva old growth and secondary forests and a neighboring patch of forest in Panama (BCI) showed similar spatial variability in biomass, basal area, and canopy light characteristics (Chave et al., 2005; Clark et al., 1996; Montgomery & Chazdon, 2001). However, this large spatial variability reduced considerably when the plot size increased to 0.25 ha (50 m × 50 m) and to approximately 10% at 1.0 ha plot size. The overall trend in the loss of spatial variability by increasing the plot size was observed in basal area in an earlier study in La Selva (Clark & Clark, 2000). The same study showed that the basal area was more variable on steep ultisol slopes than old alluvial terraces and ultisol ridgetops.

Together, these studies suggest that the small-scale variability of forest structure and biomass at pixel sizes of 10–20 m is very large. At these scales the biomass is influenced by forest disturbance and the gap dynamics that may change rapidly due to wind, tree fall, and mortality. However, at spatial resolutions greater than 0.25 ha (50 m × 50 m), forest structure and biomass start to be more stable through time and less impacted by small scale disturbance. Patterns of forest biomass over the landscape can be detected at scales larger than 0.25 ha, when the AGB follows a normal distribution (Fig. 3). In forests of La Selva, the distribution of AGB does not deviate strongly from normality or stationarity (mean and variance do not vary significantly in space) at 1.0 ha scale, suggesting that this is a suitable scale for estimating aboveground biomass. At smaller spatial resolutions, when the AGB distribution is irregular and varies significantly from normality and stationarity, estimation of AGB is subject to variable errors over the landscape.

5.2. Mapping biomass

We developed algorithms at three spatial scales of 0.25 ha, 0.5 ha, and 1.0 ha from radar backscatter measurements and the height index and applied the algorithms to the radar images at corresponding spatial resolutions of 50 m, 71 m, and 100 m. Our main objective in this analysis was to assess the performance of radar estimation of AGB

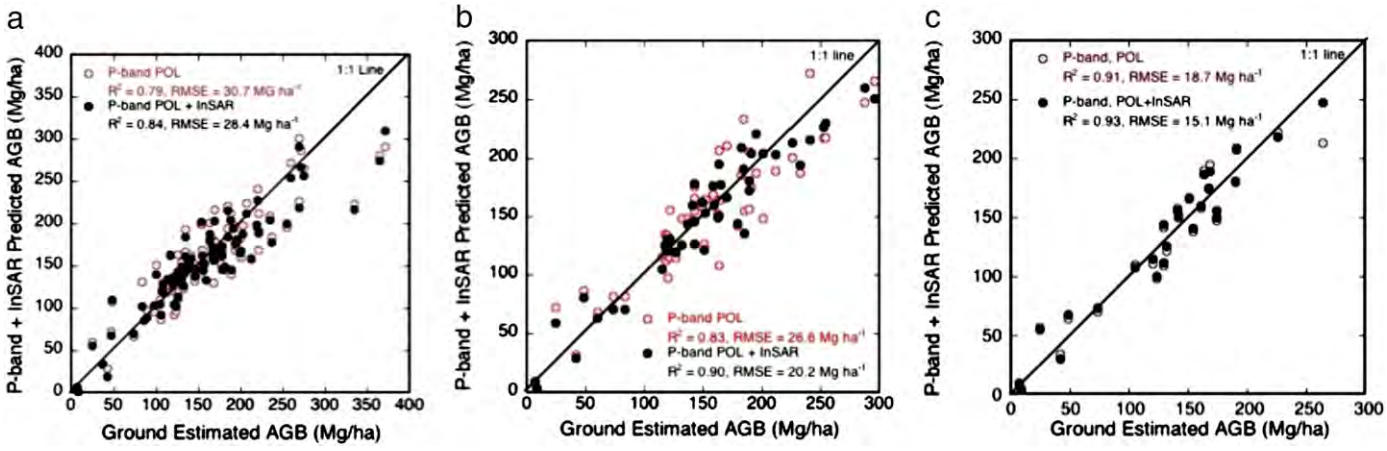

Fig. 13. Predicted vs. ground estimated aboveground biomass from P-band radar backscatter measurements at HH, HV, and VV polarizations and the InSAR derived height index at three spatial scales: a) 0.25 ha, (b) 0.5 ha, and (c) 1.0 ha.

by aggregating the spatial resolutions. We started our analysis at 50 m resolution because this was approximately the minimum spatial resolution where the forest structure at the pixel scale shows an approximate normal and stationary distribution over the landscape. By further increasing the pixel size, we reduce the speckle noise in radar backscatter measurements, which in turn, can help to reduce the estimation error. In addition, there is often a large geolocation error of approximately 10–50 m that combines the GPS (Ground Positioning System) errors associated with the location of the plots, and orthorectification errors of radar imagery. Choosing larger pixel size also reduced the errors associated with the orientation of plots with respect to the radar geometry that often causes pixels around the edge of the plots be partially covered by trees outside the plot.

The overall correlation between radar backscatter and AGB depended on the scale of observation. Both L-band and P-band polarized backscatter had better correlation with biomass measurements at 1.0 ha plots. The estimation of AGB from scale-dependent algorithms also showed an improvement in the error (RMSE) as the scale increased from 0.25 ha to 1.0 ha. In order to check the significance of the reduction of RMSE, we calculated the 95% confidence interval at all scales and for both L-band and P-band results. The confidence intervals (CI) were calculated using $CI = M \pm \frac{SE}{\sqrt{n}}$, where M is the mean value of AGB (169.7 Mg ha^{-1}), SE is the standard error, and n the number of samples. In general, for the same SE, the larger the number of samples, the smaller is the width of the confidence interval. The adjusted confidence intervals are considered an alternative to estimate the significance of accuracy improvements from the scale analysis.

At L-band, the width of the confidence interval after adjustments for the number of points was 6.25 at 1.0 ha (28 points), 6.1 at 0.5 ha (49 points), and 6.43 (92 points) at 0.25 ha. At P-band the adjusted width of the intervals were 3.7 at 1.0 ha, 3.8 at 0.5 ha, and 3.9 at 0.25 ha. These results show that as the scale of the analysis changes from 0.25 ha to 1.0 ha, the accuracy of the radar estimation improves over the same confidence intervals. Given the approximately normal distribution and stationary behavior of the forest biomass over the landscape when sampled at the 1.0 ha scale, and the improved accuracy of the radar estimation at the same scale, the results suggest that the best resolution to map the aboveground biomass of tropical forests from the radar imagery is about 100 m or greater. The spatial resolution of the biomass map also depends strongly on the radar design and its azimuth and range resolutions. In the case, of AIRSAR, operating at 40 MHz, 100 m resolution is obtained by more than 500 looks.

The results also suggested that the algorithm developed at one scale must be applied at radar images with equivalent pixel resolution. Applying algorithms developed at one scale to images at different resolution introduces errors in biomass estimation. To produce biomass maps at resolutions larger than 100 m (1.0 ha), we recommend using the 1.0 ha scale algorithm to 100 m resolution images and then aggregating the biomass pixels to produce maps at larger pixels. Fig. 14 provides a biomass map produced at 100 m resolution using the P-band polarimetric backscatter algorithm.

5.3. Implications for global forest carbon assessment

Currently, two synthetic aperture radar missions to study the forest structure and biomass are being studied by NASA and ESA. NASA's mission, DESDynl (Deformation, Ecosystem Structure and Dynamic of Ice) is an L-band SAR operating in polarimetric and repeat-pass interferometric modes and is combined with a multi-beam lidar sensor for measuring forest height (http://desdyni.jpl.nasa.gov/mission/). The BIOMASS mission is a P-band polarimetric SAR with the capability of repeat-pass Interferometry (http://www.esa.int/). Together these missions are capable of providing spatially resolved and accurate estimate of vegetation height and biomass. The performance of radar sensors in capturing the spatial variability of forest structure is a key element to unambiguously estimate the biomass or to be used in a fusion approach to extrapolate the lidar estimation of the biomass over the landscape. In this study, we have shown that the radar imagery is sensitive to forest biomass, is capable of capturing the spatial variability, and can provide estimates of aboveground biomass. However, because of the spatial variability of forest structure, the performance of the radar backscatter and height measurements are strongly dependent on the scale of observation. Over the tropical forests, where spatial variability is large, 1.0 ha (100 m × 100 m) appears to be an ideal scale for mapping the aboveground biomass. At this scale, the radar resolution of 100 m is achieved after averaging a large number of pixels (SAR multi-looking) that allows a significant reduction of speckle noise. This process also reduces orthorectification errors involved in locating the 100 m radar pixel on the ground. As expected, radar sensors at P-band perform better than L-band in estimating the aboveground biomass over a larger range. The overall biomass range (the so-called saturation referred to in radar literature) for each frequency depends on the sensitivity of radar, the calibration of the radar measurements, and the accuracy of the estimation. In this study, we have shown that at L-band, using all polarized backscatter measurements, the range can reach somewhere between 150 and 200 Mg ha^{-1}. However, estimation error can be large enough that only one (AGB>100 Mg ha^{-1}) or two (AGB>100 and AGB>150 Mg ha^{-1}) levels of biomass can be estimated unambiguously. At P-band however, the sensitivity extended to biomass values of 300 Mg ha^{-1} at 1.0 ha scale. The P-band estimation of AGB was accurate to approximately 15 Mg ha^{-1} averaged over the entire range of biomass at La Selva. The results indicate that at both frequencies, additional information such as the forest height obtained from radar Interferometry or lidar measurements can improve both the range of biomass estimation and the overall accuracy. It is expected that future fusion approaches integrating measurements from radar and lidar sensors can provide global forest biomass at spatial resolutions of approximately 1.0 ha or larger.

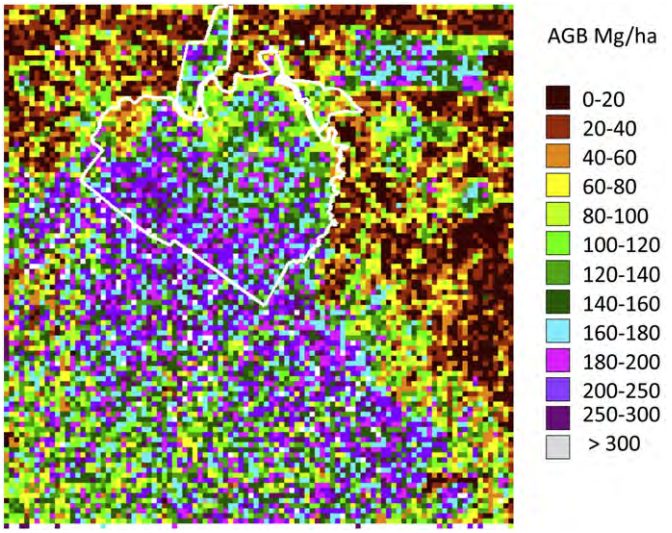

Fig. 14. Distribution of aboveground biomass derived from P-band radar backscatter algorithm based on HH, HV, and VV polarized backscatter measurements at 1.0 ha resolution.

6. Conclusions and recommendations

Despite numerous studies to estimate forest biomass from radar imagery, there are very few examples in the literature that address the impact of forest structural variability and radar measurement

geometry on aboveground biomass estimation. The paucity of forest inventory data at various plot sizes that can adequately sample the landscape and provide detailed structural information has impeded the necessary spatial analyses. Using forest inventory plots over a range of biomass values from early succession to old growth tropical forests in La Selva, Costa Rica, allowed us to examine the spatial variability of forest structure and quantify its impact on the L-band and P-band radar estimation of AGB. We showed that at both frequencies, the best results are obtained at spatial scales where the distribution of AGB over the landscape is both stationary and normal and the radar resolution is large enough to reduce the speckle noise and the geolocation error between radar pixel and the plot location. Although, the spatial variability of forest biomass approaches the normality and stationarity at scales greater than 0.25 ha (50 m × 50 m), the radar estimation of biomass can be significantly improved at 1.0 ha scale (100 m × 100 m pixel size). Only when the spatial resolution is about 100 m, can errors associated with the biomass estimation from radar backscatter or height measurements be reduced to acceptable levels (10–20%) for mapping the aboveground biomass globally.

The loss of sensitivity of radar backscatter to aboveground biomass and hence the accuracy of the estimation also depends on the spatial scale. In this study, the combined L-band polarized backscatter estimated biomass up to 100 Mg ha^{-1} with about 15% accuracy at 1.0 ha scale. We found higher values of biomass could be estimated with larger errors or by adding forest height index up to 200 Mg ha^{-1}. At P-band, the combined polarized backscatter estimated biomass with approximately 10% accuracy up to 300 Mg ha^{-1} at 1.0 ha scale. Adding forest height index improved the biomass estimation over the entire range and reduced the errors associated with high biomass values.

Future spaceborne radar measurements at L-band and P-band measurements by DESDynl and BIOMASS are accompanied with accurate estimates of forest height and vertical profiles from lidar measurements. Fusion approaches that can integrate measurements from both radar and lidar sensors are necessary to successfully map vegetation three-dimensional structure and biomass globally. The development of these approaches depends on several factors: 1. A theoretical understanding of the nature of radar and lidar measurements of forest structure. 2. The relationship between forest structure and biomass for different forest types. 3. Spatial variability of forest structure and the required sampling frequency and spatial scale in mapping the biomass. 4. Development of methodologies that can fuse spatially contiguous measurements from radar imagery with sparse sampling of lidar from space.

Acknowledgements

This work was performed partially at the Jet Propulsion Laboratory, California Institute of Technology, under contract from National Aeronautic and Space Administration and the support of NASA's Terrestrial Ecology Program. We would like to thank the NASA AIRSAR crew for the acquisition of the radar images and the JPL airborne SAR group for processing and calibration of the data. We thank Dr. Ralph Dubayah and Bryan Blair and Michele Hofton for their help for processing the LVIS data. Our special thanks also go to the La Selva Biological Station, the Organization for Tropical Studies, and the Carbono Project (funded by DOE, NSF and the Andrew W. Mellon Foundation).

References

Baker, T. R., Phillips, O. L., Malhi, Y., Almeida, S., Arroyo, L., DiFiore, A., et al. (2004). Variation in wood density determines spatial patterns in Amazonian forest biomass. *Global Change Biology*, *10*(5), 545–562.

Blair, J. B., Rabine, D. L., & Hofton, M. A. (1999). The Laser Vegetation Imaging Sensor (LVIS): A medium-altitude, digitization-only, airborne laser altimeter for mapping vegetation and topography. *ISPRS Journal of Photogrammetry and Remote Sensing*, *54*, 115–122.

Brown, S. (1997). *Estimating biomass and biomass change of tropical forests: A primer. UN-FAO Forestry Paper 134* Rome, Italy.

Chave, J., Chust, G., Condit, R., Aguilar, S., Perez, R., & Lao, S. (2005). Error propagation and scaling for tropical forest biomass estimates. In O. L. Phillips, & Y. Malhi (Eds.), *Tropical forests and global atmospheric change* (pp. 155–163): Oxford University Press.

Chave, J., Condit, R., Lao, S., Caspersen, J. P., Foster, R. B., & Hubbell, S. P. (2003). Spatial and temporal variation in biomass of a tropical forest: Results from a large census plot in Panama. *Journal of Ecology*, *91*, 240–252.

Chazdon, R. L. (1996). Spatial heterogeneity in tropical forest structure: canopy palms as landscape mosaics. *Trends in Ecology and Evolution*, *11*, 8–9.

Chazdon, R. L., Redondo Brenes, A., & Vilchez Alvarado, B. (2005). Effects of climate and stand age on annual tree dynamics in tropical second-growth rain forests. *Ecology*, *86*, 1808–1815.

Clark, D. B. (1990). La Selva Biological Station: A blueprint for stimulating tropical research. In A. Gentry (Ed.), *Four neotropical forests* (pp. 9–27): Yale University Press.

Clark, D. B., & Clark, D. A. (2000). Landscape-scale variation in forest structure and biomass in a tropical rain forest. *Forest Ecology and Management*, *137*, 185–198.

Clark, D. B., Clark, D. A., & Read, J. M. (1998). Edaphic variation and the mesoscale distribution of tree species in a neotropical rain forest. *Journal of Ecology*, *86*, 101–112.

Clark, D. B., Clark, D. A., Rich, P. M., Weiss, S., & Oberbauer, S. F. (1996). Landscape-scale evaluation of understory light and canopy structure: Methods and application to a neotropical lowland rain forest. *Canadian Journal of Forest Research*, *26*(5), 747–757.

Denslow, J. S., & Hartshorn, G. S. (1994). Tree-fall gap environments and forest dynamic processes. In L. A. McDade, K. S. Bawa, H. A. Hespenheide, & G. S. Hartshorn (Eds.), *La Selva: Ecology and natural history of a neotropical rain forest* (pp. 120–127). Chicago: University of Chicago Press.

Dixon, R. K., Brown, S. A., Houghton, R. A., Solomon, A. M., Trexler, M. C., & Wisniewski, J. (1994). Carbon pools and flux of global forest ecosystems. *Science*, *263*, 185–190.

Dobson, M. C., Ulaby, F. T., Pierce, L. E., Sharik, T. L., Bergen, K. M., Kellndorfer, J., et al. (1995). Estimation of forest biophysical characteristics in Northern Michigan with SIR-C/X-SAR. *IEEE Transactions on Geoscience and Remote Sensing*, *GE-33*, 877–895.

Drake, J. B., Dubayah, R. O., Clark, D. B., Knox, R. G., Blair, J. B., Hofton, M. A., et al. (2002). Estimation of tropical forest structural characteristics using large-footprint lidar. *Remote Sensing of Environment*, *79*, 305–319.

Drake, J. B., Knox, R. G., Dubayah, R. O., Clark, D. B., Condit, R., Blair, J. B., et al. (2003). Aboveground biomass estimation in closed canopy Neotropical forests using lidar remote sensing: Factors affecting the generality of relationships. *Global Ecology & Biogeography*, *vol. 12*. (pp. 147–159).

Dubayah, R. O., & Drake, J. B. (2000). Lidar remote sensing for forestry. *Journal of Forestry*, *98*, 44–46.

Guariguata, M. R., Chazdon, R. L., Denslow, J. S., Dupuy, J. M., & Anderson, L. (1997). Structure and floristics of secondary and old-growth forest stands in lowland Costa Rica. *Plant Ecology*, *132*, 107–120.

Holdridge, L. R., Grenke, W. C., Hatheway, W. H., Liang, T., & Tosi, J. A. J. (1971). *Forest environments in tropical life zones: A pilot study*. New York, NY: Pergamon.

Isaaks, E. H., & Srivastava, R. M. (1989). *An Introduction to applied geostatistics*. Oxford University Press, NY.

Laurance, W. F., Fearnside, P. M., Laurance, S. G., Delamonica, P., Lovejoy, T. E., Rankin-de Merona, J., et al. (1999). Relationship between soils and Amazon forest biomass: A landscape-scale study. *Forest Ecology and Management*, *118*, 127–138.

Lefsky, M. H., D.J., Keller, M., Camargo, P. B., Cohen, W. B., Carabajal, C. C., et al. (2005). Estimates of forest canopy height and aboveground biomass using ICESat. *Geophysical Research Letters*, *32*, L22S02.

McDade, L. A., Bawa, K. S., Hespenheide, H. A., & Hartshorn, G. S. (1994). *La Selva: ecology and natural history of a Neotropical rain forest.* Chicago: University of Chicago Press.

Menalled, F. D., Kelty, M. J., & Ewel, J. J. (1998). Canopy development in tropical tree plantations: A comparison of species mixtures and monocultures. *Forest Ecology and Management*, *104*, 249–263.

Montgomery, R. A., & Chazdon, R. L. (2001). Light gradient partitioning by tropical tree seedlings in the absence of canopy gaps. *Oecologia*, *131*, 165–174.

Nicotra, A. B., Chazdon, R. L., & Iriarte, S. V. B. (1999). Spatial heterogeneity of light and woody seedling regeneration in tropical wet forests. *Ecology*, *80*, 1908–1926.

Oberbauer, S. F., Clark, D. B., Clark, D. A., Rich, P. M., & Vega, G. (1993). Light environment, gas exchange, and annual growth of saplings of 3 species of rainforest trees in Costa Rica. *Journal of Tropical Ecology*, *9*, 511–523.

Perry, D. A. (1994). *Forest ecosystems.* Baltimore, Maryland: Johns Hopkins University Press.

Ranson, K. J., & Sun, G. (1994). Mapping biomass for a northern forest using multifrequency SAR data. *IEEE Transactions on Geoscience and Remote Sensing*, *32* (3), 388–396.

Rich, P. M., Clark, D. B., Clark, D. A., & Oberbauer, S. F. (1993). Long-term study of solar radiation regimes in a tropical wet forest using quantum sensors and hemispherical photography. *Agricultural and Forest Meteorology*, *65*, 107–127.

Richards, P. W. (1996). *The tropical rain forest* (2nd edn.). Cambridge: Cambridge University Press.

Russell, A. E., Fisher, R. F., & Raich, J. W. (2007). Tree species effects on soil properties in experimental plantations in tropical moist forest. *Soil Science Society of America*, *71*, 1389–1397.

Saatchi, S., Despain, D., Halligan, K., Crabtree, R., & Yu, Y. (2007). Estimating forest fire fuel load from radar remote sensing. *IEEE Geoscience and Remote Sensing*, *45*, 1726–1740.

Saatchi, S., & Moghaddam, M. (2000). Estimation of crown and stem water content and biomass of boreal forest using polarimetric SAR imagery. *IEEE Transactions on Geoscience and Remote Sensing*, *38*, 697–709.

Sarabandi, K., & Lin, Yi-cheng (2000). Simulation of interferometric SAR response for characterizing the scattering phase center statistics of forest canopies. *IEEE Transactions on Geoscience and Remote Sensing*, *38*(1), 115–125.

Ulaby, F. T., Moore, R. K., & Fung, A. K. (1982). Microwave Remote Sensing: Active and Passive, Vol. II — Radar Remote Sensing and Surface Scattering and Emission Theory, Addison-Wesley, Advanced Book Program, Reading, Massachusetts, 609 pp.

Zebker, H. A., & Villasenor, J. (1992). Decorrelation in interferometric radar echoes. *IEEE Transactions on Geoscience and Remote Sensing*, *30*(5), 950–959.